# High-temperature phase transitions in incommensurate $Rb_2WO_4$



2000 J. Phys.: Condens. Matter 12 9307

(http://iopscience.iop.org/0953-8984/12/44/311)

J. Phys.: Condens. Matter **12** (2000) 9307–9315. Printed in the UK PII: S0953-8984(00)16713-X

# High-temperature phase transitions in incommensurate $Rb_2WO_4$

A Jorio†, P Saint-Grégoire‡ and M A Pimenta†

† Departamento de Física, Universidade Federal de Minas Gerais, Caixa Postal 702, 30123-970, Belo Horizonte, Minas Gerais, Brazil

‡ LMMI, Université de Toulon et du Var, BP 132, 83957 La Garde Cédex, France

Received 30 August 2000

**Abstract.** Raman experiments were performed on $Rb_2WO_4$ crystals, between room temperature and 850 K, including the high-temperature incommensurate phase. The experimental results observed in the incommensurate ($T_I = 746$ K) and the lock-in ($T_C = 660$ K) phase transitions can be explained by an order–disorder apex model, where the gradual *up/down* ordering of the $WO_4^{2-}$ apexes is responsible for the structural changes. The as-grown sample exhibits a monoclinic–orthorhombic phase transition that is suppressed by heat treatment of the sample, and this result is confirmed by differential scanning calorimetry measurements.

## 1. Introduction

The appearance of incommensurate phases in crystals of the $A_2BX_4$ family has been observed and extensively studied [1, 2]. In the majority of the $A_2BX_4$ crystals, the incommensurate modulation is along the pseudo-hexagonal $c$-axis and is given by $q = (m/n + \delta)c^*$. The high-temperature phase generally belongs to the orthorhombic $Pmcn$ ($D_{2h}^{16}$) space group with four formula units per unit cell ($Z = 4$). The low-temperature commensurate phase (lock-in phase) appears when the modulation locks in at a commensurate value ($\delta \to 0$) and the crystal generally assumes a monoclinic ($C_{2h}$ point group) or an orthorhombic ($C_{2v}$ point group) structure. For these compounds, the incommensurate transition occurs below $T = 600$ K and the best-known examples are $K_2SeO_4$ and $Rb_2ZnCl_4$ [1].

There is another class of $A_2BX_4$ compounds in which the incommensurate phase occurs at higher temperatures ($T > 590$ K) [2, 3]. In this case, the high-temperature phase belongs to the hexagonal space group $P6_3/mmc$ ($D_{6h}^4$, $Z = 2$), where the $BX_4^{2-}$ tetrahedra exhibit a full orientational disorder related to the vertical *up/down* orientation of their apexes. In this case, the incommensurate modulation is associated with the probability of finding the $BX_4^{2-}$ tetrahedra in an *up* or *down* vertical orientation, and the wave vector lies in the basal plane of the hexagonal structure [2, 3]. The lock-in phase transition is related to the *up/down* ordering of the tetrahedra, and the commensurate phase has an orthorhombic $Pmcn$ symmetry.

Basal-plane incommensurate modulation is known to occur in alkali molybdates and tungstates like $K_2MoO_4$, $K_2WO_4$, and $Rb_2WO_4$ [2, 3]. Although these crystals exhibit interesting properties compared with the well studied $A_2BX_4$ incommensurate compounds (e.g. $K_2SeO_4$ and $Rb_2ZnCl_4$), there are few experimental studies devoted to these compounds [4–10], probably due to their highly hygroscopic character.

0953-8984/00/449307+09$30.00  

$Rb_2WO_4$ exhibits a hexagonal $P6_3/mmc$ ($D^4_{6h}$, $Z = 2$) structure in the high-temperature phase I, with $a = 6.568(6)$ Å and $c = 8.411(8)$ Å, at 768 K [5, 6]. The incommensurate transition occurs at about $T_I = 740$ K, and it is characterized by a basal-plane modulation given by $q = (\frac{1}{2} + \delta)b^*$ (phase II). At about $T_C = 660$ K, $\delta$ jumps to zero and the lock-in commensurate phase III takes place, with an orthorhombic $Pmcn$ symmetry, and a doubled unit cell ($a = 6.506(6)$ Å, $b = 11.34(1)$ Å, and $c = 8.219(5)$ Å, at $T = 618$ K) [5, 6]. A recent differential scanning calorimetry (DSC) experiment [10] showed that these two phase transitions exhibit a strong order–disorder character, related to the vertical *up/down* ordering of the $WO_4^{2-}$ tetrahedra. Furthermore, it was shown that the crystal exhibits a rare first-order incommensurate phase transition, which has been explained by the coupling between the tetrahedra orientation and crystal elasticity [10]. Kools *et al* [4] proposed that the room temperature phase has a monoclinic symmetry ($C2/m$ space group) with $a = 12.841(2)$ Å, $b = 6.285(1)$ Å, $c = 7.854(1)$ Å, and $\beta = 115.82(1)^\circ$. According to van den Berg *et al* [6], the monoclinic–orthorhombic phase transition occurs at $T_L = 568$ K.

In this work we have studied the high-temperature phase transitions in $Rb_2WO_4$ crystal by Raman scattering. We identified the symmetry for the Raman-active modes and our experimental results give support for the *up/down* order–disorder apex model [3, 10] for the incommensurate and lock-in phase transitions. Also, it is shown that the reported monoclinic–orthorhombic phase transition [4, 6] is related to the presence of water molecules in the crystalline lattice ($Rb_2WO_4{\cdot}xH_2O$), and this phase transition is suppressed by heat treatment of the sample. DSC and thermogravimetric analysis (TGA) experiments support this conclusion.

## 2. Experimental procedure

Colourless single crystals of $Rb_2WO_4$ were grown by slow evaporation of an aqueous solution at room temperature. The samples were prepared in a glove box with a dry nitrogen atmosphere, due to the highly hygroscopic nature of the material.

Raman experiments were performed using a triple-monochromator spectrometer (DILOR-XY) equipped with multi-array (GOLD) and CCD detectors, using the green line ($\lambda = 514.5$ nm) of an argon laser (COHERENT INNOVA 70). A $0.5 \times 0.2 \times 0.1$ mm$^3$ monocrystal was encapsulated in a quartz tube, for air humidity isolation. The measurements were performed from room temperature up to 850 K, between 25 cm$^{-1}$ and 1200 cm$^{-1}$.

The DSC experiment was performed on a 47.18 mg powder sample using a Mettler-TA3000 device. Seven heating/cooling cycles were performed between room temperature and 820 K. Temperature change rates of 5 and 10 K min$^{-1}$ were used. The measurements were performed in a nitrogen atmosphere in order to protect the sample against air humidity.

A TGA experiment was performed in order to investigate the loss of mass during the heating of the sample. A 12.24 mg monocrystal sample was measured using a SDT (simultaneous differential techniques) device. The sample was heated up to 800 K under a $N_2$ atmosphere and the temperature change rate was 5 K min$^{-1}$.

## 3. Results and discussion

Figure 1 shows the Raman spectra of the as-grown $Rb_2WO_4$ crystal in the room temperature monoclinic phase, using the scattering geometries $x(yy)\bar{x}$, $x(zz)\bar{x}$, and $x(yz)\bar{x}$† (the sample

† This is the notation of S P S Porto, where the letters outside the parentheses give the propagation direction of the incident and scattered light, and the letters inside the parentheses give the polarization direction of the incident and scattered light.

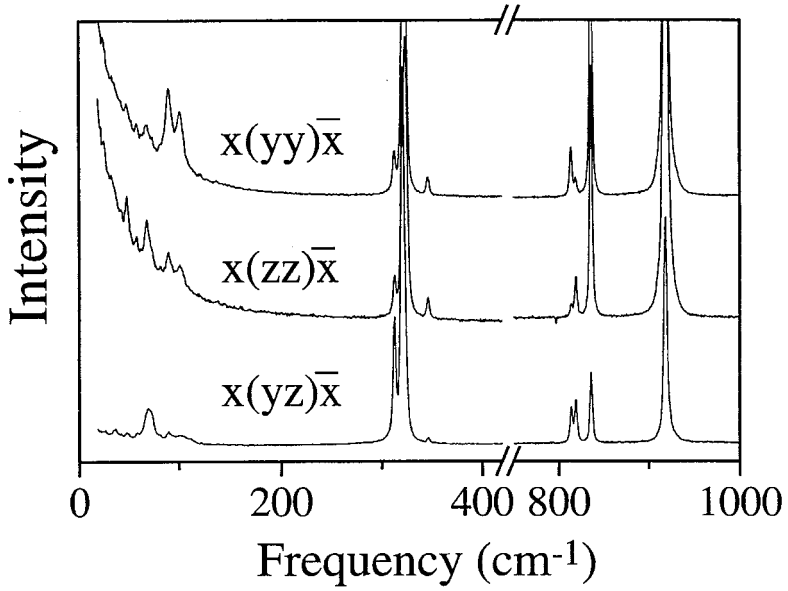


**Figure 1.** Room temperature Raman spectra of the as-grown $Rb_2WO_4$ sample in three different scattering geometries.

orientation was previously determined by x-ray diffraction). Note that the Raman bands are separated into three spectral regions; the peaks below 100 $cm^{-1}$ are related to the external modes, the peaks between 300 $cm^{-1}$ and 350 $cm^{-1}$ are related to the $\nu_2$ and $\nu_4$ bending internal modes, and the peaks related to the $\nu_1$ and $\nu_3$ stretching internal modes are found between 800 $cm^{-1}$ and 950 $cm^{-1}$. The spectra were fitted by a sum of Lorentzian curves and the frequency of each mode is displayed in table 1 (the assignment of the symmetric—$\nu_1$ and $\nu_2$—and the anti-symmetric—$\nu_3$ and $\nu_4$—modes in table 1 will be discussed later). The number of observed internal modes is in agreement with a monoclinic $C2/m$ structure, where one $\nu_1$, two $\nu_2$, three $\nu_3$, and three $\nu_4$ internal modes are expected for the $xx$, $yy$, $zz$ ($A_g$ irreducible representation), and $yz$ ($B_g$ irreducible representation) scattering polarizations [11]. It is interesting to observe that the frequencies of the $A_g$ and $B_g$ modes practically coincide. The crystalline anisotropy manifests itself by changes in the relative intensity of the Raman peaks, principally for those associated with the external modes and the $\nu_3$ modes (see figure 1).

**Table 1.** Room temperature $Rb_2WO_4$ Raman frequencies ($cm^{-1}$) before and after heat treatment.

| As-grown sample | | | | | | | | |
|---|---|---|---|---|---|---|---|---|
| External modes | 48 | 57 | 71 | 91 | 101 | | | |
| Internal modes | $\nu_4$ | $\nu_2$ | $\nu_2'$ | $\nu_4'$ | $\nu_3$ | $\nu_3'$ | $\nu_3''$ | $\nu_1$ |
| | 315 | 324 | 327 | 350 | 817 | 822 | 839 | 921 |
| Heat-treated sample | | | | | | | | |
| External modes | 42 | 61 | 91 | 121 | | | | |
| Internal modes | $\nu_4$ | — | $\nu_2'$ | $\nu_4'$ | $\nu_3$ | — | $\nu_3''$ | $\nu_1$ |
| | 308 | — | 328 | 340 | 813 | — | 865 | 927 |

Excluding the Rayleigh wing at low frequencies, which is more intense for the parallel scattering geometries, the high-temperature spectra obtained with the three different scattering geometries are very similar. Figure 2 shows the dependence on temperature for the Raman frequencies and damping constants obtained with the cross-polarized $x(yz)\bar{x}$ geometry. The external modes region (below 100 $cm^{-1}$) was fitted considering the same number of Lorentzian curves as for the room temperature spectrum, all of them with the same damping constant. We can observe in figure 2 that the Raman spectra show considerable changes at about 490 K, rather than at the reported monoclinic phase transition temperature $T_L = 568$ K [6]. The damping constants of all vibrational modes increase significantly and the frequencies of several modes exhibit discontinuities, stronger for the $\nu_4$ and $\nu_4'$ modes; above $T = 490$ K, only two $\nu_3$ and one $\nu_2$ modes are observed (see figure 2), in agreement with an orthorhombic $D_{2h}^{12}$ structure, where one $\nu_1$, one $\nu_2$, two $\nu_3$, and two $\nu_4$ internal modes are expected for the $xx$, $yy$, $zz$ ($A_g$ irreducible representation), and $yz$ ($B_{3g}$ irreducible representation) scattering polarizations [11].

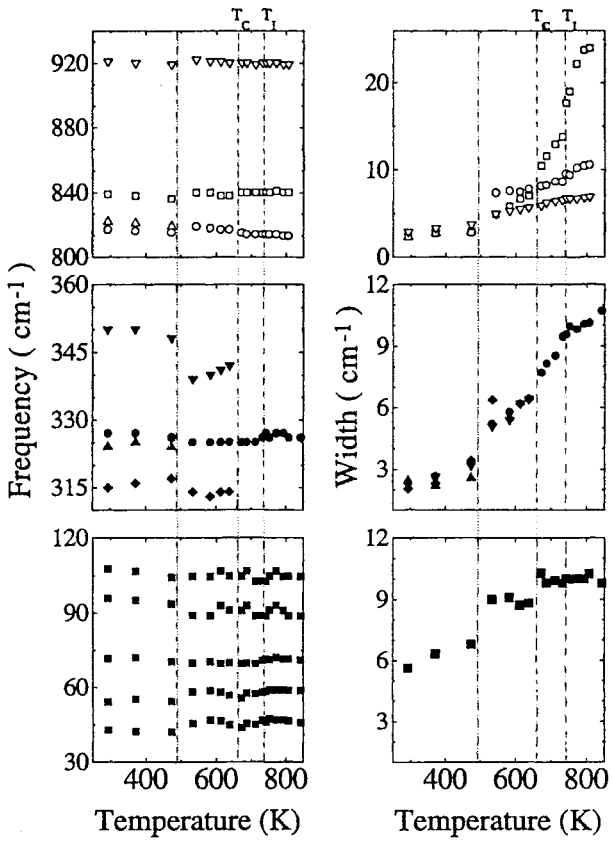


**Figure 2.** Temperature evolution for the Raman frequencies and damping constants of the as-grown $Rb_2WO_4$ sample, using the $x(yz)\bar{x}$ scattering geometry. The external modes were fitted with a unique value for the damping constants. ▽: $\nu_1$; □: $\nu_3''$; △: $\nu_3'$; ○: $\nu_3$; ▼: $\nu_4'$; ●: $\nu_2'$; ▲: $\nu_2$; ♦: $\nu_4$; ■: external modes.

The lock-in ($T_C$) and the incommensurate ($T_I$) phase transitions manifest themselves in the Raman experiment by a discontinuous increase of the internal mode damping constants (see figure 2). This result is evidence of the order–disorder character of these phase transitions, in agreement with previous DSC results [10]. The broadening is strong for the $\nu_3''$ mode

($\sim$839 cm$^{-1}$; see figure 2), and it is of interest to understand why this phenomenon is stronger for this special mode. The $\nu_3$ modes in a *Pmcn* structure of the $A_2BX_4$ crystals consist of displacements of the B and X atoms along one of the three crystallographic directions [12]. The direction of the atomic displacements, and the relative phases for the vibrations of the four $BX_4^{2-}$ groups in the unit cell, determine the irreducible representation associated with each mode. By using group theory projectors [12] it is easy to establish that, in the orthorhombic phase, the two Raman-active $\nu_3$ modes belonging to the $A_g$ irreducible representation exhibit atomic displacements along $\boldsymbol{z}$ and $\boldsymbol{y}$, respectively. The same conclusion is valid for the two Raman-active $\nu_3$ modes belonging to the $B_{3g}$ irreducible representation. The two Raman-active $\nu_3$ modes belonging to the $B_{1g}$ and $B_{2g}$ irreducible representations exhibit atomic displacements along $\boldsymbol{x}$. Therefore, the two $\nu_3$ modes observed above $T = 490$ K ($\nu_3$ and $\nu_3''$ in table 1 and figure 2) have atomic displacements along $\boldsymbol{y}$ and $\boldsymbol{z}$, respectively, since we have investigated the $yy$, $zz$ ($A_g$), and $yz$ ($B_{3g}$) polarized spectra.

Below the monoclinic–orthorhombic phase transition, the $A_g$ and the $B_{1g}$ modes of the orthorhombic structure belong to the same $A_g$ irreducible representation of the $C_{2h}$ point group, and the $B_{2g}$ and the $B_{3g}$ modes of the orthorhombic structure belong to the same $B_g$ irreducible representation of the $C_{2h}$ point group. Therefore, the $\nu_3$ modes with atomic displacements along $\boldsymbol{x}$ also appear in the $zz$-, $yy$-, and $yz$-polarized spectra. Since the crystal exhibits a pseudo-hexagonal structure, it is reasonable to expect that the $\nu_3$ modes with atomic displacements along $\boldsymbol{x}$ and $\boldsymbol{y}$ will exhibit similar frequencies. This result leads us to conclude that the higher-frequency $\nu_3''$ (see table 1, figures 1 and 2) mode is that one with atomic displacements along the pseudo-hexagonal $z$-axis, and the two lower-frequency $\nu_3$ and $\nu_3'$ modes observed below 490 K (see table 1, figures 1 and 2) are those with atomic displacements along $\boldsymbol{x}$ and $\boldsymbol{y}$. The fact that the broadening occurs mostly for the internal modes, and that it is stronger for the $\nu_3''$ internal mode characterized by atomic displacements along the pseudo-hexagonal $z$-axis direction supports the order–disorder apex model proposed for the incommensurate and lock-in phase transitions [3, 10], where the gradual *up/down* ordering of the $WO_4^{2-}$ apexes directed along the $z$-direction is responsible for the structural changes.

The lock-in phase transition is also accompanied by the appearance of two $\nu_4$ peaks below $T_C$, in agreement with the symmetry lowering. It is interesting to observe that no peaks appear below the incommensurate phase transition. The Raman spectra in the incommensurate phase are quite similar to those of the high-temperature disordered hexagonal phase. This result seems to be related to the order–disorder character of the incommensurate modulation. The partial ordering of the tetrahedra orientation in the incommensurate phase does not distort the $WO_4^{2-}$ tetrahedra significantly and, therefore, no internal modes appear below $T_I$ [12]. Although the two phase transitions are of first order with large entropy jumps [10], structural transformations are more significant below the lock-in phase transition, where the modulation vector locks in at $q = \frac{1}{2}b^*$.

After heating up to 850 K, the sample was left at high temperature for a few hours, and then it was cooled down to room temperature. Figure 3 shows the Raman spectra of the internal modes at room temperature, before and after the heat treatment. Note that the room temperature spectrum after heating is different from that of the as-grown sample. Table 1 displays the frequency of all Raman modes at room temperature after and before heat treatment. The frequencies of most of the peaks are different after and before the heating cycle. Furthermore, for the heat-treated sample, only one $\nu_2$ and two $\nu_3$ modes (see figure 3) are observed, in agreement with an orthorhombic symmetry. These results strongly suggest that the monoclinic–orthorhombic phase transition is suppressed when the sample is heat treated at high temperatures ($\sim$850 K), and this result was confirmed by a DSC experiment, as discussed below.

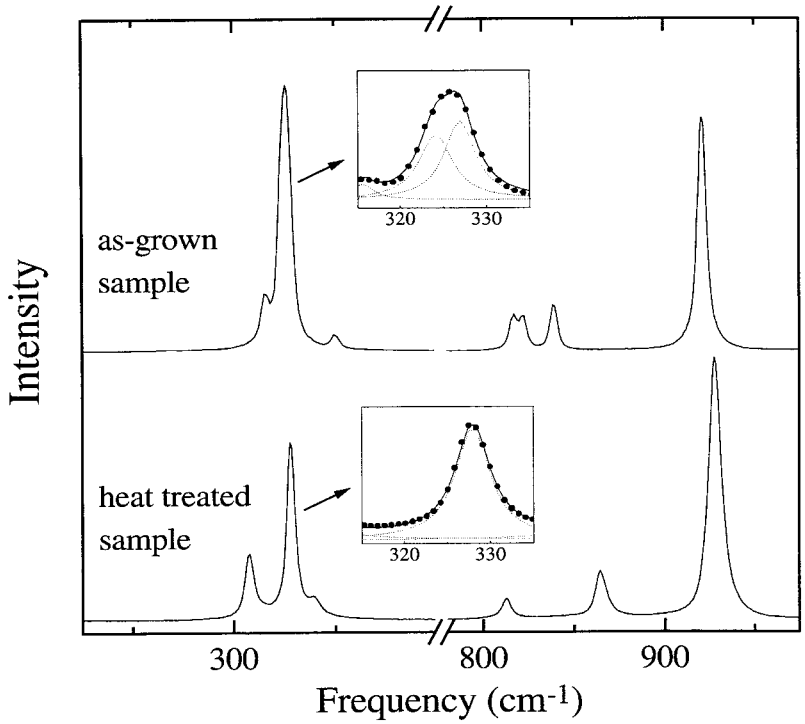


**Figure 3.** Room temperature $x(yz)\bar{x}$ Raman spectra of the as-grown and heat-treated $Rb_2WO_4$ samples, in the region of the internal modes.

Figure 4 shows the DSC thermograms between room temperature and 800 K obtained in four thermal cycles. In the first DSC heating cycle we can observe two sharp anomalies at about $T_C = 660$ K and $T_I = 746$ K, related, respectively, to the lock-in and the incommensurate phase transitions (the transition temperatures are determined by the onset of the DSC peaks), and an anomalous broad feature between 380 K and 570 K. Note that the higher temperature of this broad feature corresponds approximately to the temperature of the monoclinic phase transition $T_L = 568$ K proposed by van den Berg *et al* [6]. In the second heating, the anomalous broad feature transformed into a well defined peak at 490 K, in agreement with Raman results (see figure 2). Repeating the same heating/cooling process, the intensity of the peak at 490 K decreased (see the third run in figure 4) and disappeared completely (see the fourth run in figure 4). After the heat treatment, the DSC thermogram exhibits only the two reversible enthalpy anomalies, at $T_C = 660$ K and $T_I = 746$ K, in agreement with reference [10].

It is well known that the $Rb_2WO_4$ crystal is highly hygroscopic. Considering that the sample studied was grown by slow evaporation of an aqueous solution, we propose that the thermal anomalies observed in the first heating between 380 K and 570 K, and the orthorhombic–monoclinic phase transition observed at $T = 490$ K (second and third DSC heating curves in figure 4 and Raman results in figure 2) are related to the presence/departure of water molecules in the as-grown sample ($Rb_2WO_4 \cdot xH_2O$). In order to clarify the DSC results we performed a thermogravimetric analysis (TGA) experiment which allows the observation of sample mass changes at high temperatures, related to the loss of water. Figure 5 shows the TGA curves for the first and the second heating of the sample up to 800 K. The change of mass is given in per cent of the mass at the beginning of each heating measurement. In the

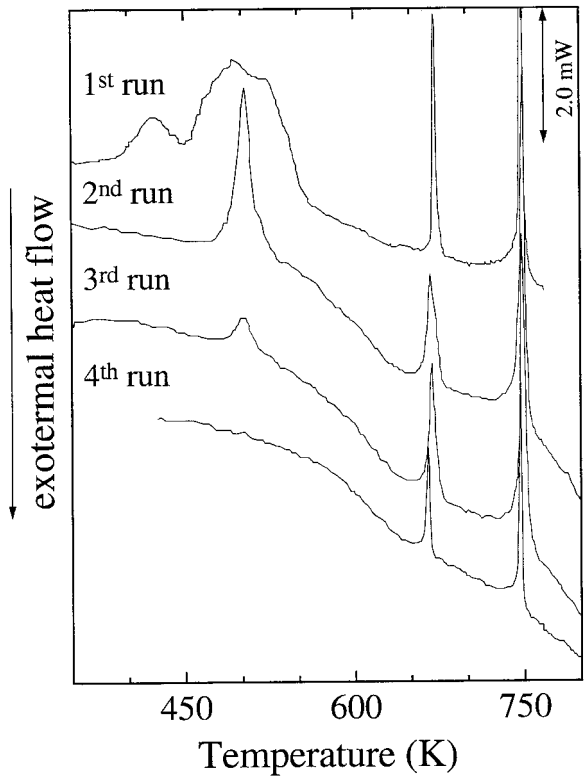


**Figure 4.** First to fourth heating DSC thermograms of a 47.18 mg powder sample of $Rb_2WO_4$. The fourth thermogram was obtained with the rate of 5 K $min^{-1}$, while the three others were obtained with the rate 10 K $min^{-1}$.

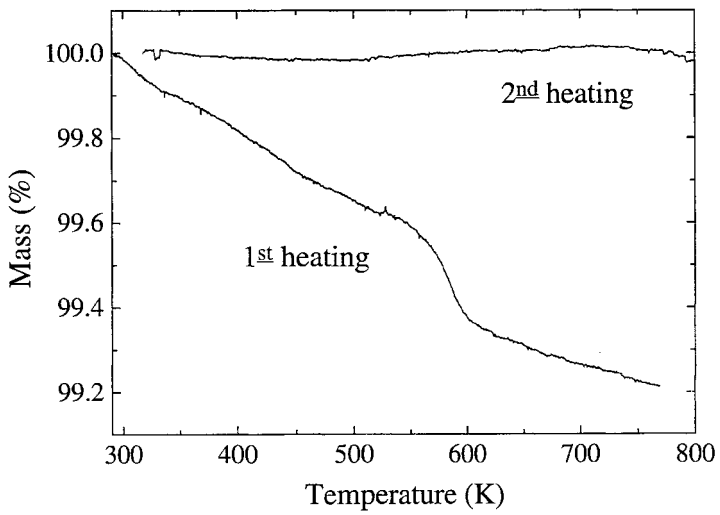


**Figure 5.** TGA curves for the first and the second heating of an initially 12.24 mg as-grown $Rb_2WO_4$ sample, up to 800 K. The change of mass is given in per cent of the mass at the beginning of each heating.

first heating the sample loses 0.8% of its mass and the TGA curve exhibits an abrupt decrease around $T_L$. The sample was left at high temperature for a few hours, and then it was cooled down to room temperature (TGA measurements were not performed during this time). On the second heating, the sample started with 99.0% of the initial mass (1% of the sample mass corresponds approximately to one molecule of water per unit cell), and no loss of mass was observed, with the device precision of $\pm 0.02\%$.

Summarizing, the DSC experiment shows that the anomaly near the reported monoclinic–orthorhombic phase transition disappears upon heat treatment of the sample; the TGA experiment shows a decrease of the sample mass, compatible with the loss of water at high temperatures; the Raman experiment shows that the room temperature spectra of the as-grown and heat-treated samples are different, with the number of internal modes observed in the first one compatible with the monoclinic symmetry, and the number of modes observed in the second one compatible with the orthorhombic symmetry. Therefore, we conclude that the monoclinic–orthorhombic phase transition is suppressed when the sample is heat treated at high temperature ($\sim$800 K) due to the departure of water.

In order to clarify the influence of water molecules in the lattice dynamics, the sample used in the Raman experiment was removed from the quartz tube that protected it against air humidity, and Raman spectra were taken during the time interval in which the crystal absorbs water. Figure 6 shows that the most important changes in the spectrum taken 120 s after exposing the sample to air humidity are the appearance of the 822 $cm^{-1}$ $\nu_3'$ mode, the appearance of the 839 $cm^{-1}$ $\nu_3''$ mode, and the frequency upshift of the $\nu_4$ mode around 308 $cm^{-1}$. Note that these features are also observed in the room temperature spectrum of the as-grown sample, showing that the crystal tends to regenerate the monoclinic structure after absorbing water. The intensities of the $\nu_3$ and $\nu_4$ peaks decrease with respect to those of the $\nu_1$ and $\nu_2$ peaks,

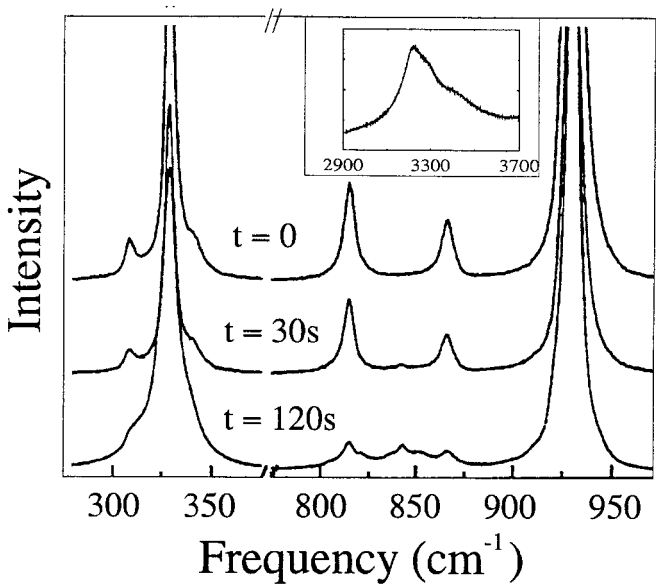


**Figure 6.** Raman spectra of an initially anhydrous $Rb_2WO_4$ sample as a function of the time of exposure to air humidity, using the $x(yz)\bar{x}$ scattering geometry. The spectra were obtained with 5 s accumulation. The inset shows a broad band at about 3300 $cm^{-1}$, typical for the presence of water [13].

indicating that the $WO_4^{2-}$ molecules start to become free, since the $\nu_3$ and $\nu_4$ modes are not Raman active for the free tetrahedra (this result allows us to assign the symmetrical and anti-symmetrical internal modes, as shown in table 1). The inset to figure 6 shows a broad band at about 3300 $cm^{-1}$, typical for the presence of water [13], measured during the time that the crystal was exposed to the air humidity.

## 4. Conclusions

$Rb_2WO_4$ belongs to a class of $A_2BX_4$ compounds where the incommensurate phase appears at high temperature. The as-grown sample has a monoclinic $C2/m$ symmetry at room temperature due to the presence of water molecules in the crystal lattice ($Rb_2WO_4{\cdot}xH_2O$) that breaks the orthorhombic symmetry. Raman and DSC experiments show that a heat treatment of the sample at ~800 K restores fully the anhydrous orthorhombic structure. The DSC thermograms of the heat-treated sample exhibit enthalpy anomalies only at the incommensurate ($T_I$) and lock-in ($T_C$) phase transitions. The room temperature Raman spectra of the heat-treated sample are different from that of the as-grown sample, and consistent with the orthorhombic symmetry. Therefore, the anhydrous $Rb_2WO_4$ crystal exhibits, above room temperature, the $Pmcn$–incommensurate–$P6_3/mmc$ sequence of phase transitions.

The incommensurate and lock-in $Rb_2WO_4$ phase transitions exhibit an order–disorder character, where the gradual *up/down* ordering of the $WO_4^{2-}$ apexes directed along the pseudo-hexagonal $z$-axis is responsible for the structural changes of the lattice. The broadening of the Raman internal modes at these phase transitions, stronger for the $\nu_3''$ mode, in which the atomic displacements take place along $z$-direction, gives support for this order–disorder apex model.

## Acknowledgments

The authors would like to acknowledge R L Moreira for very helpful discussions, R A Silva for performing the TGA experiment, and A M Moreira for technical assistance in the DSC experiment. One of us (A Jorio) is grateful to the Brazilian Agencies CAPES and CNPq. This work was supported by grants from the Brazilian Agencies FAPEMIG and FINEP.

## References

[1] Cummins H Z 1990 *Phys. Rep.* **185** 211
[2] Kurziński M 1995 *Acta Phys. Pol.* B **26** 1101
[3] Luk'yanchuk I, Jorio A and Pimenta M A 1998 *Phys. Rev.* B **57** 5086 and references therein
[4] Kools F X N M, Koster A S and Reick G D 1970 *Acta Crystallogr.* B **26** 1974
[5] van den Akker A W M, Koster A S and Rieck G D 1970 *J. Appl. Crystallogr.* **3** 389
[6] van den Berg A J, Tuinstra F and Warczewski J 1973 *Acta Crystallogr.* B **29** 586
[7] Warczewski J 1979 *Phase Transitions* **1** 131
[8] Tuinstra F and van den Berg A J 1983 *Phase Transitions* **3** 275
[9] van den Berg A J, Overeijnder H and Tuinstra F 1983 *Acta Crystallogr.* C **39** 678
[10] Luk'yanchuk I, Jorio A and Saint-Grégoire P 2000 *Phys. Rev.* B **61** 3147 and references therein
[11] Jório A, Dantas M S S, Pinheiro C B, Speziali N L and Pimenta M A 1998 *Phys. Rev.* B **57** 203
[12] Jorio A, Echegut P, Speziali N L and Pimenta M A 1999 *Phys. Rev.* B **59** 11 251
[13] Herzberg G 1945 *Infrared and Raman Spectra of Polyatomic Molecules* (New York: Van Nostrand)